Upper Bound Estimates of Fruit Reachability in Orchard Trees using Linear Motion

Stavros Vougioukas*, Rajkishan Arikapudi, Joshua Munic

Department of Biological and Agricultural Engineering, University of California - Davis, Davis, CA 95616, USA

* Corresponding author. Email: svougioukas@ucdavis.edu

Abstract

Prototype robotic fruit harvesters typically utilize multiple degree-of-freedom (DOF) arms. The working hypothesis is that as tree branches constrain fruit reachability, redundancy is necessary to navigate through branches and reach fruits inside the canopy. However, modern commercial orchards increasingly adopt trees of SNAP architectures (Simple, Narrow, Accessible, and Productive). This paper presents simulation estimates of linear fruit reachability (LFR) for high-density, trellised pear and cling peach trees. Individual fruit LFR is defined as a Boolean variable that is zero if the fruit's geometric projection along an approach direction vector results in collision with a branch; otherwise, it is one; linear only motion is considered for reaching fruits. The simulations used digitized geometric tree models and fruit locations. The calculated LFRs are averaged of individual fruit LFRs and constitute upper-bound estimates of the true LFRs, i.e., they are optimistic, because the tree models included only branches thicker than approximately 2.5 cm. Multiple 'harvesting passes' were simulated for each type of trees, in the sense that the *k*th-pass LFR of the fruits remaining on the trees were calculated after all reachable fruits were removed in the previous *k*-1 passes. Results showed that 92.2% of the pears and 97% of the cling peaches were linearly reachable after five "harvesting passes" at appropriate, optimal approach angles. The LFRs decreased monotonically - exponentially - as a function of the number of passes, thus indicating a diminishing return after more than three sets of approach angles were implemented. The first-pass LFR of cling peaches was significantly larger than that of pears, which can be attributed to simpler canopy and better fruit positioning. These preliminary results indicate that for some trees of SNAP-type architectures fruit reachability may not require complex and expensive arms with many degrees of freedom.

Keywords: Agriculture, trees, computer, simulation, robotics, harvesting.

1. Introduction

Fresh market tree fruit harvesting is one of the most labor-intensive operations incurring high cost and dependence on a large seasonal semi-skilled workforce. Existing shake-and-catch harvesters cause excessive damage and their use has been restricted mainly to fruits harvested for juice or processing. Selective harvesting (i.e., robotic) technologies for fresh market fruits have also not been developed to the point where they can be used commercially. Robust, accurate and efficient fruit detection, localization and detachment pose significant technical challenges. Two major obstacles for adoption, which are not exclusively related to perception or grasping, are very low fruit picking efficiency and throughput. These two harvesting performance metrics have been identified as the most important variables (along with purchase price) that define harvest cost (Harrell, 1987). Based on reported results from an extensive literature review, Bac et al., (2016) calculated an average fruit picking cycle equal to 33 s per fruit, and an average harvest success rate equal to 66% for robot prototypes developed so far. Although these numbers are averages over radically different crops, ranging from eggplants to citrus, and very diverse robot designs, they are indicative of the problem. Per comparison, a tree fruit or strawberry picker can pick at ten times this rate.

The performance of a robotic harvester depends on the interrelationships among orchard layout, tree canopy structures and spatial fruit distributions with robot mechanics. For tree fruit harvesting, low performance is, to a large extent, the combined result of several factors. Fruit visibility is of course a very important one, but even if perception were perfect, performance would still be limited by fruit accessibility, and by complex, time-consuming motion planning (e.g., Schuetz et al., 2014) and control algorithms (e.g., Mehta & Burks, 2014). Such algorithms are needed because robotic fruit harvester prototypes typically utilize manipulators with many DOFs. The hypothesis is that, as branches constrain fruit reachability, high kinematic dexterity is necessary to navigate through branches and reach fruits inside the canopy (e.g., van Henten et al., 2010). This is true for many crops. In fruit orchards, however, growers are increasingly adopting high-density SNAP (Simple, Narrow, Accessible, and Productive) tree architectures (Karkee & Zhang, 2012). Such orchards feature narrow almost two-dimensional canopies (e.g., tall and super spindle apple orchards) that create "fruiting walls", which are easier to harvest manually, either with ladders or with orchard platforms (Gallardo & Brady, 2015).

This paper presents simulation studies that estimate bounds of fruit reachability on trellised SNAP-type Bartlett pear trees and parallel-V cling peach trees using linear only motion (e.g., linear, telescopic arms). Spherical type robots have been developed and tested by researchers in the past (e.g., Harrell, Adsit, Slaughter, 1985). Their use in traditional orchard architectures could not achieve picking efficiency and throughput that justified commercialization. The goal of this work is to define linear fruit reachability metrics and to use geometric models of orchard trees and the locations of all

their fruits to investigate how fruit reachability changes as a function of approach direction, when several directions are used in a sequential fashion. The approach direction is defined by the combination of azimuth and elevation approach angles. A range of approach directions is explored for each pass, in order to find the best one(s). Our long-term vision is that such information can be used for the design of robotic harvesters that feature simpler (cheaper, faster) arms, albeit a large number of them. Also, such studies could potentially guide canopy shaping and fruit thinning strategies, thus leading to approaches that treat the trees and robots as a system that needs to be co-designed and co-optimized.

2. Materials and Methods

2.1. Trees and Fruit Positions Digitization and Modelling

A large-volume digitization system was developed that utilizes electromagnetic field for data acquisition (Arikapudi et al., 2015)). A PowerTRAK 360TM digitizer (Polhemus, Colchester, VT, USA) was used to manually digitize points on tree surfaces with an RMS accuracy of 0.2 cm. The PowerTRAK 360TM sensor connects via cable to a G4 'Hub' module; this module transmits digitized data via Radio Frequency (RF) to an RF module connected to the computer via USB. A 'Source' module generates the electromagnetic field required to track the sensor. The precision and accuracy of the devices were calculated via experimentation; the sensor had precision and accuracy better than 1 cm when the tracking volume was about 1.5 m x 1.5 m x 1.5 m from the source. The digitizer was designed specifically for pear and cling-peach trees. The maximum volume of such trees in commercial orchards in California is 3 m x 4.5 m x 4.5 m. To digitize such trees at an accuracy and precision better than 1 cm, 18 sources are needed because each source can cover a volume of 1.5 m x 1.5 m x 1.5 m. The sources should be placed at appropriate locations to cover the entire volume of an individual tree. To achieve this, a frame was built for the digitization process so that the sources were moved within the frame in sequence to cover the whole tree volume. Six sources were used to speed up the digitization process of each side of a tree (volume of 1.5 m x 3 m x 4.5 m). Since the sensor used for data collection was based on the interaction of magnetic fields created by the G4 source and the field created by the Power Track 360TM the workspace should be free of metal to ensure the tracked volume had no interference. So, the frame that was built was made of wood and plastic to mitigate error in the collected data. The digitization process followed the following procedure for data acquisition.

Figure 1. A wooden frame carried six digitizer 'source' modules, in order to cover the volume of large trees.

Tree architecture was defined by its trunk, number of main branches, sub-branches, sub-sub-branches, and so on. Each of these branches was divided further into segments such that each segment was approximately straight. The architectural information of the tree was saved with each of the segment during data collection. Branches that were thin enough to be flexible (< 2.5 cm) were not digitized, as they do not present obstacles to the movement of robotic harvesters; hence, they do not limit reachability. After the entire tree was digitized, the surface of each segment was approximated with a conical frustum.

2.2. Linear Fruit Reachability

Consider the coordinate system of Fig. 1, and a unit vector **d** defined by two angles: an azimuth/yaw angle, α, about the z-axis, and an elevation/pitch angle, θ, around the x axis. Elevation is -90^o along the –z axis and 90^o along the z axis. Azimuth ranges from -90 ^{o} to 90 ^{o} and it is defined as 0^o along the y axis; it increases clockwise. Individual fruit reachability is defined as a Boolean variable that is zero if the fruit's geometric projection along the approach direction vector **d** results in collision with a branch; otherwise, it is one. This definition corresponds to linear motion, if an actuator

were used to pick the fruits, so we refer to it as "linear reachability". Fruit-with-fruit collisions are not included in this definition of reachability, because in a real harvesting scenario a fruit occluding other fruits along **d** would be picked first, since it would be closer to the robot arm on the 'harvesting' side; therefore it would not present an obstacle. Linear fruit reachability *LFR*(**d**) is defined as the total number of linearly reachable fruits on a number of trees along a particular approach direction **d,** divided over the total number of trees.

We also define *LFR*($\mathbf{d}_1$; $\mathbf{d}_2$; …; $\mathbf{d}_{i-1}$; $\mathbf{d}_i$) as the linear fruit reachability for the *i*th "harvesting pass" along a direction $\mathbf{d}_i$, as the linear fruit reachability of the fruits remaining on the tree, after fruits that were reachable along vectors $\mathbf{d}_1$, $\mathbf{d}_2$, …, $\mathbf{d}_{i-1}$ were removed. Finally, we define the cumulative linear fruit reachability *CLFR*($\mathbf{d}_1$, $\mathbf{d}_2$, …, $\mathbf{d}_K$) as the total number of fruits that were linearly reachable after K consecutive "harvesting passes". By definition:

$$CLFR(\mathbf{d}_1,\mathbf{d}_2,\ \ldots,\mathbf{d}_K) = LFR(\mathbf{d}_1) + LFR(\mathbf{d}_1;\mathbf{d}_2) + \ \ldots\ + LFR(\mathbf{d}_1;\mathbf{d}_2;\ldots;\mathbf{d}_k) \quad (1)$$

A key observation is that since according to our definition fruit reachability is not affected by other fruits, the order of the "harvesting passes" does not affect the cumulative *CLFR*. Obviously, the calculation of *LFR*(**d**) requires fast collision detection between fruits and branches. In this work, an open-source physics engine called *Bullet Physics Library* was used to model the trees and fruits and run the simulations. The fruit geometric projections were calculated implicitly: the gravity vector was set along **d**, and each fruit was let to 'fall' toward each harvesting side of the tree. The physics engine integrated the fruit motion under this gravity, and invoked its internal collision detection functions at each integration time step ($1/60^{th}$ of a second). If a fruit-branch collision occurred, it was reported and the fruit's linear reachability along **d** was set to zero.

3. Results and Discussion

3.1. LFR for High-Density Pear Trees

A total of ten trellised Bartlett pear trees (*Pyrus communis* 'Williams pear') were digitized; the total number of fruits was 1890.

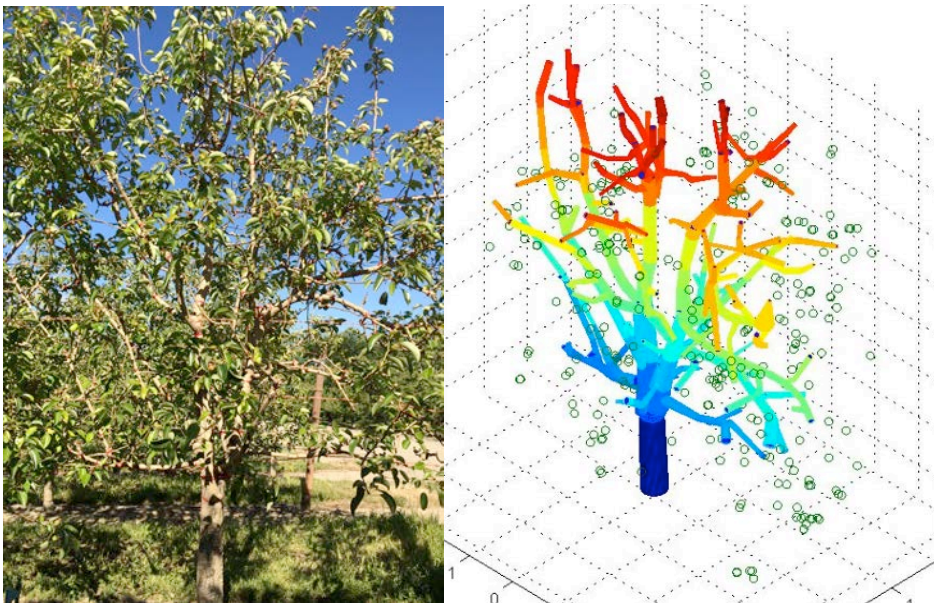

Figure 2. High-density Bartlett pear tree (left) and geometric model of reconstructed tree (right); segments are represented as frustums and dimensions are in feet.

Given the asymmetrical shape of pears, it was assumed that fruits would be picked by grasping their spherical bottom part; hence, LFR was calculated using the spherical part of the pears. The value used for the average diameter of this part of the fruits was 6.5 cm, which corresponds to size at 120 days after bloom (Mitcham and Elkins, 2007) and to the typical minimum picking size. The elevation angle for the approach direction $\mathbf{d}_1$ ranged from -90° (actuator would approach from below the canopy) to 90° (actuator approach from above the canopy) with a step of 10°. The azimuth angle ranged from -90° to 90° with a step of 10°. Fig. 3 shows a map of *LFR*($\mathbf{d}_1$).

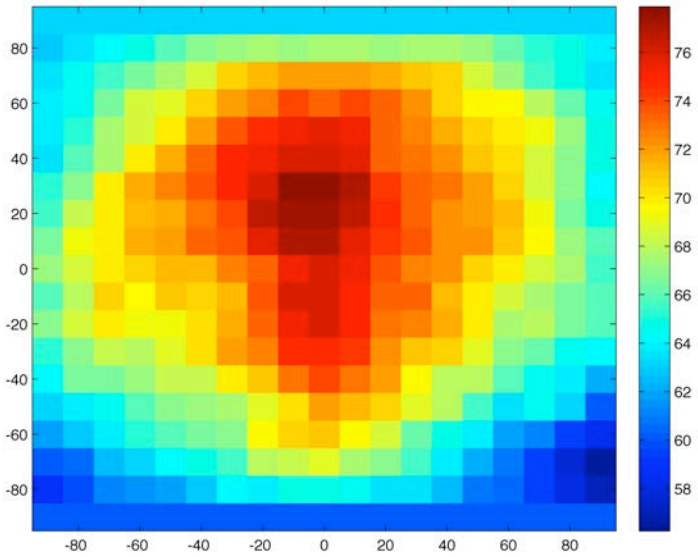

Figure 3. Linear fruit reachability $LFR(\mathbf{d}_1)$ as a function of elevation and azimuth angles (y and x axis respectively).

The maximum LFR corresponds to the optimal approach vector, $\mathbf{d}_1^*$. This value was calculated to be $LFR(\mathbf{d}_1^*) = 77.9\%$ and was achieved from an elevation angle equal to 30^o and azimuth angle at 0^o. It corresponds to 1472 reachable pears out of 1890 in total, on the ten trees. The darker region close to the center of the image implies that if the particular trees were to be harvested using linear actuators, they would offer better accessibility to their fruits from directions above the horizontal plane and close to a right angle with respect to the orchard row.

Next, $LFR(\mathbf{d}_1^*; \mathbf{d}_2)$ for a second "harvesting pass" was calculated. The 1472 reachable pears from the first pass were removed from the trees, and reachability was calculated for the remaining fruits. The azimuth angle ranged again from -90^o to 90^o with a step of 10^o. Fig. 4 shows a map of the second-pass $LFR(\mathbf{d}_1^*; \mathbf{d}_2)$. As expected, the minimum second-pass LFR was 0% at the direction of first-pass $LFR(\mathbf{d}_1^*)$. The maximum second-pass $LFR(\mathbf{d}_1^*;\mathbf{d}_2^*)$ was 10.2% and was achieved from an elevation angle equal to 50^o and azimuth angle at 80^o. This maximum $LFR(\mathbf{d}_1^*;\mathbf{d}_2^*)$ corresponds to 192 reachable pears out of 1890 fruits in total, and out of 418 fruits remaining on the tree after the first pass (45.9%). The maximum number of linearly reachable fruits with the two passes combined was 1664, i.e., $CLFR(\mathbf{d}_1^*,\mathbf{d}_2^*) = 88.0\%$. One remark is that *LFR*s ranging from 9.2% to 9.9% could be achieved from various azimuth and pitch angles, as it can be seen from the regions of dark red pixels left and right in Fig. 4.

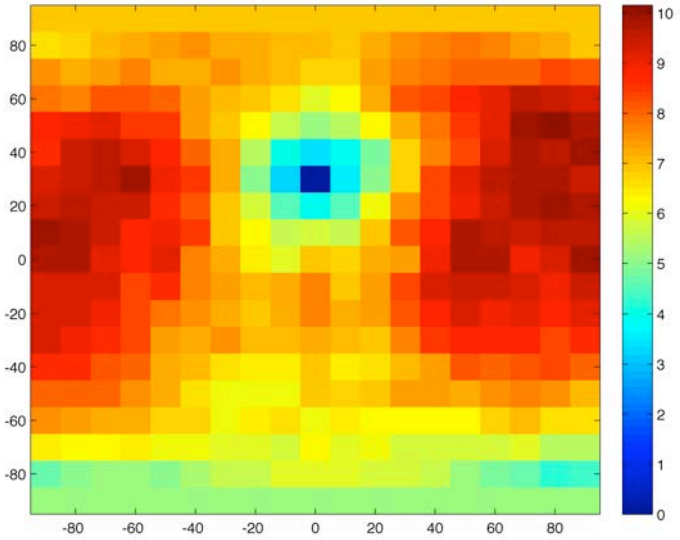

Figure 4. Second-pass $LFR(\mathbf{d}_1^*; \mathbf{d}_2)$ as a function of elevation and azimuth angles (y and x axis respectively).

It was also verified that the order of the "harvesting passes" did not affect the cumulative *CLFR*, i.e., $CLFR(\mathbf{d}_1^*,\mathbf{d}_2^*) = CLFR(\mathbf{d}_2^*,\mathbf{d}_1^*)$.

Three more passes were implemented. The maximum *LFR*s for the 3rd, 4rth and 5th pass were 3.6%, 0.42%, and 0.11% respectively (Fig. 5). These *LFR*s correspond to 68, 8 and 2 fruits respectively. The maximum number of linearly reachable fruits with the five passes combined was 1742, i.e., $CLFR(\mathbf{d}_1^*,\mathbf{d}_2^*,\mathbf{d}_3^*,\mathbf{d}_4^*,\mathbf{d}_5^*) = 92.2\%$.

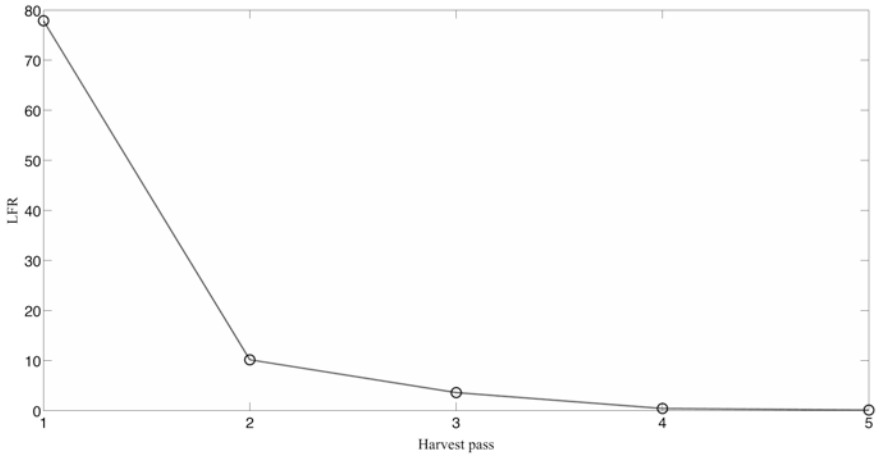

Figure 5. *LFR* as a function of harvest pass.

3.2. LFR for High-Density V-Shaped Cling Peach Trees

Twenty high-density V-shaped cling peach trees (*Prunus persica* 'Dr. Davis) and the positions of all their size appropriate fruits (5120 in total) were digitized.

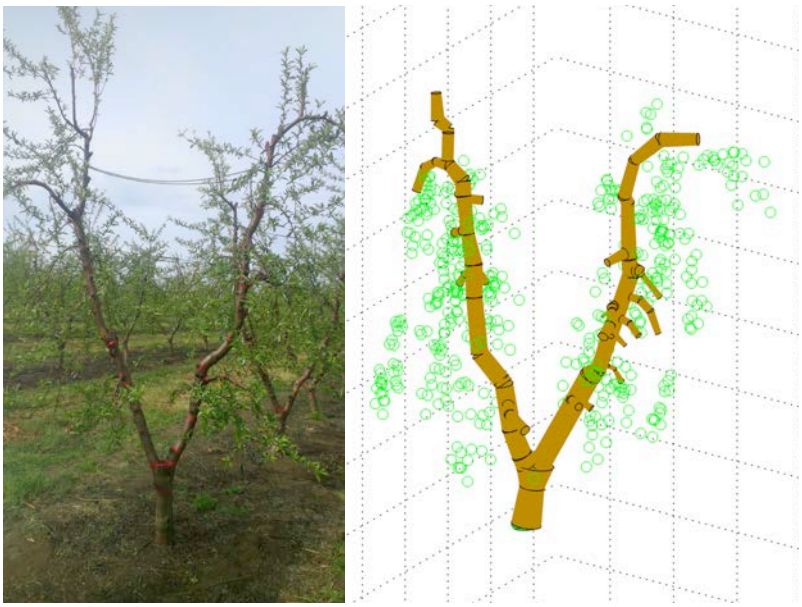

Figure 6. High-density V-shaped cling peach trees (left) and geometric model of reconstructed tree (right); segments are represented as frustums and dimensions are in feet.

Five harvesting passes were simulated for these trees. The elevation angle for the approach direction $\mathbf{d}_1$ ranged from -90° (actuator would approach from below the canopy) to 90° (actuator approach from above the canopy) with a step of 10°. The azimuth angle ranged from -90° to 90° with a step of 10°. The value used for the average diameter of the fruits was 4.3 cm. The corresponding *LFR*s were 91.82%, 4.73%, 0.45%, 0.02% and 0% and corresponded to 4701, 242, 23 and 0 cling peach fruits. The reduction of *LFR* as a function of harvest-pass was again exponential, just like in the pear trees. The maximum first-pass $LFR(\mathbf{d}_1^*)$ was achieved from an elevation angle equal to -10° and azimuth angle at 10°, as

can be seen from Fig. 7. The maximum first-pass *LFR* for the cling peach trees was 18% higher than that of the pear trees. This was a combined result of less complex canopy and better positioning of the fruits, for the peach tree. The maximum number of linearly reachable fruits with the five passes combined was 4967, i.e., CLFR($\mathbf{d}_1^*,\mathbf{d}_2^*,\mathbf{d}_3^*,\mathbf{d}_4^*,\mathbf{d}_5^*$) = 97%.

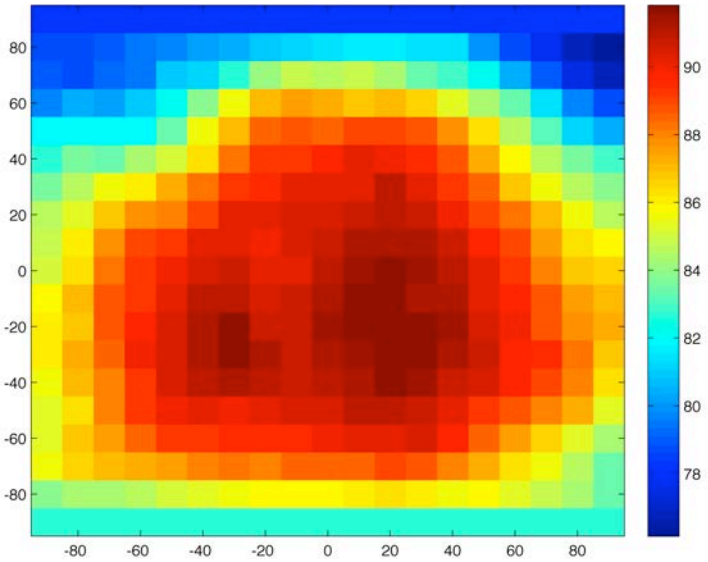

Figure 7. *LFR*($\mathbf{d}_1$) as a function of elevation and azimuth angles (y and x axis respectively).

4. Conclusions

This paper presented a simulation study on linear fruit reachability for high-density, trellised pear trees; linear only motion was used to reach the fruits. The simulation results based on the digitized geometric tree models and fruit locations showed that 92.2% of the pears and 97% of the cling peaches were reachable via linear-only motion, after five "harvesting passes", when proper approach angles were used. This implies that for some trees of SNAP-type architectures fruit reachability may not require complex and expensive arms with many degrees of freedom. Of course, thin, flexible branches were not included in this study and their effects would need to be evaluated. Also, fruit visibility does not enter at all in this analysis, and best approach directions for kinematic reachability may be very different from directions that optimize fruit visibility. Another remark is that the maximum *LFR* of each pass dropped monotonically - exponentially - as a function of the number of harvest passes. This implies that in a physical embodiment of such a harvesting system, there is a diminishing return as more approach angles are implemented; hence, trade-offs would need to be considered.

Acknowledgements

We would like to thank numerous California growers for letting us gather data during their busy harvesting season. This work was partly funded by USDA-NIFA Grant 2016-67021-24532.

References

Arikapudi, R., Vougioukas, S., Saracoglu, T. (2015). Orchard tree digitization for structural-geometrical modelling. In Proceedings of the 10th European Conference on Precision Agriculture (ECPA), pp. 329 – 336, Volcani Center, Israel.

Bac, C.W., Henten, E.J., Hemming, J. and Edan, Y., 2014. Harvesting Robots for High-value Crops: State-of-the-art Review and Challenges Ahead. Journal of Field Robotics, 31(6), 888-911.

Gallardo, R.K. and Brady, M.P., 2015. Adoption of labor-enhancing technologies by specialty crop producers: The case of the Washington apple industry. Agricultural Finance Review, 75(4), 514-532.

Harrell, R.C., Adsit, P.D., Slaughter, D.C. 1985. Real-time vision-servoing of a robotic tree fruit harvester. ASAE Paper 85-3550, St. Joseph, MI 49085, USA.

Karkee, M. and Zhang, Q., 2012. Mechanization and automation technologies in specialty crop production. Resource Magazine, 19(5), 16-17.

Mehta, S.S. and Burks, T.F., 2014. Vision-based control of robotic manipulator for citrus harvesting. Computers and Electronics in Agriculture, 102,146-158.

Mitcham, E. J., Elkins, R. B. 2007. Pear Production and Handling Manual, Chapter 11, pp. 77. University of California, Agriculture and Natural Resources, Communication Services. Publication 3483, Oakland, CA, USA.

Harrell, R.C., Adsit, P.D. and Slaughter, D.C., 1985. Real-time vision-servoing of a robotic tree-fruit harvester. ASAE paper 85-3550.

Schuetz, C., Baur, J., Pfaff, J., Buschmann, T. and Ulbrich, H., 2015, May. Evaluation of a direct optimization method for trajectory planning of a 9-DOF redundant fruit-picking manipulator. In Proceedings of IEEE International Conference on Robotics and Automation (ICRA), pp. 2660-2666.

Van Henten, E.J., Schenk, E.J., Van Willigenburg, L.G., Meuleman, J. and Barreiro, P., 2010. Collision-free inverse kinematics of the redundant seven-link manipulator used in a cucumber picking robot. Biosystems Engineering, 106(2), pp.112-124.

This template was updated on April 25, 2016